Reports

Tilt Precursors before Earthquakes on the San Andreas Fault, California

Abstract. *An array of 14 biaxial shallow-borehole tiltmeters (at 10^{-7} radian sensitivity) has been installed along 85 kilometers of the San Andreas fault during the past year. Earthquake-related changes in tilt have been simultaneously observed on up to four independent instruments. At earthquake distances greater than 10 earthquake source dimensions, there are few clear indications of tilt change. For the four instruments with the longest records (> 10 months), 26 earthquakes have occurred since July 1973 with at least one instrument closer than 10 source dimensions and 8 earthquakes with more than one instrument within that distance. Precursors in tilt direction have been observed before more than 10 earthquakes or groups of earthquakes, and no similar effect has yet been seen without the occurrence of an earthquake.*

Systematic tilting of the earth's crust near active faults prior to earthquakes has long been expected (*1*) but not yet observed. Recent observations (*2, 3*) and suggestions of either dilatancy-type behavior (*4*) or dislocation-type behavior (*5*) as part of the earthquake process imply a particular form of tilt change in both space and time just prior to an earthquake. We have installed a dense array of 14 biaxial tiltmeters to search for these effects along the section of the San Andreas fault that is currently most active. At least three of these tiltmeters have now been operating for almost a year. We report here observations from these three instruments which indicate that changes in tilt direction are a normal occurrence before moderate earthquakes in this region. Results from other instruments with shorter data bases indicate that similar effects occur (*6*).

Our measurement system consists of 14 biaxial shallow-borehole tiltmeters (*7*) operating at an initial sensitivity of 10^{-7} radian. They are installed about 6 km apart, about 2 m deep (*8*), and from 1 to 4 km from the fault at carefully selected sites having approximately radially symmetric topography. In general, the sites are on alternate sides of the fault, although in several cases instruments have been positioned on opposite sides of the fault. The array runs from Mt. Madonna (36°59′N, 121°42′W) to Dry Lake (36°29′N, 121°05′W) and should provide precise surface deformation data for any moderate to large earthquakes. During the past 40 years, 10 earthquakes with local magnitude (M_L) > 5 have occurred in this region, the last (M_L = 5.1) on 24 February 1972 at Bear Valley. Prior to installation of the instruments, tests were conducted on the stability, linearity, and calibration of the instruments (*9*). The data at present are recorded at the site but soon will be recorded via digital telemetry to the National Center for Earthquake Research at Menlo Park.

Since the first instrument was installed in July 1973, more than 50 earthquakes with $M_L > 2.5$ have occurred in the general region of the present network. Of these, 26 earthquakes have occurred since July 1973, with at least one instrument closer than 10 earthquake source dimensions (10 *S*) (*10*) and 8 earthquakes with more than one instrument within that distance. We have carefully checked the tilt records for the times of these earthquakes and can make the following important though preliminary observations on the general form of the data:

1) We see no indication of very rapid tilt change in the period range of seconds to hours just prior to earthquakes which could indicate rapid nonlinear deformation.

2) Few clear indications of permanent tilts or reversible tilt change (other than the passage of seismic waves) have been seen for earthquakes at distances greater than approximately 10 *S*. Following the method of Thatcher and Hanks (*10*), for $M_L = 3.0$ 10 *S* is approximately 10 km, for $M_L = 4.0$ it is 30 km, and for $M_L = 5.0$ it is 100 km for San Andreas earthquakes.

3) During aseismic periods slow sys-

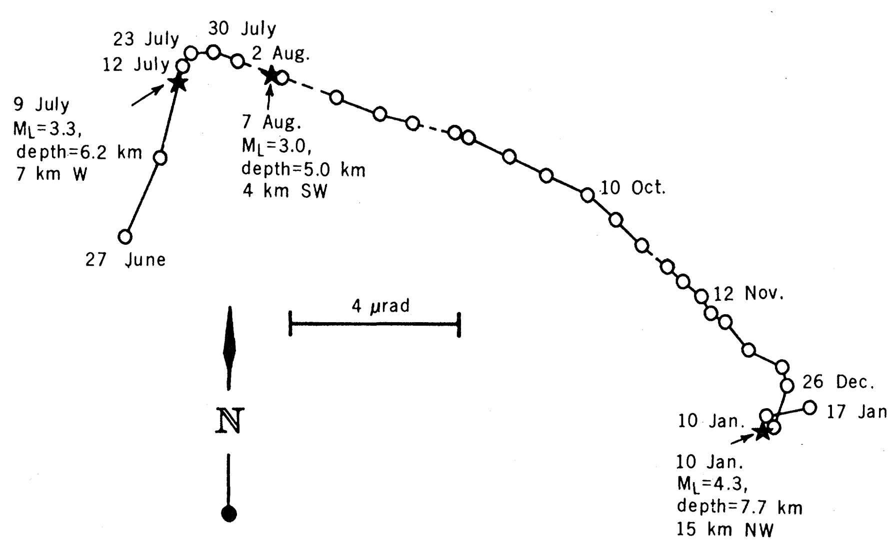

Fig. 1. Cumulative weekly mean tilt vectors (circles) from 27 June 1973 to 17 January 1974 for the Nutting site, 7 km southwest of Hollister. Tilts toward the north and east are along the positive ordinate and abscissa, respectively. Local earthquakes are also indicated (stars).

Scoreboard for Reports: In the past few weeks the editors have received an average of 63 Reports per week and have accepted 11 (17 percent). We plan to accept about 10 Reports per week for the next several weeks. In the selection of papers to be published we must deal with several factors: the number of good papers submitted, the number of accepted papers that have not yet been published, the balance of subjects, and length of individual papers.

Authors of Reports published in *Science* find that their results receive good attention from an interdisciplinary audience. Most contributors send us excellent papers that meet high scientific standards. We seek to publish papers on a wide range of subjects, but financial limitations restrict the number of Reports published to about 12 per week. Certain fields are overrepresented. In order to achieve better balance of content, the acceptance rate of items dealing with physical science will be greater than average.

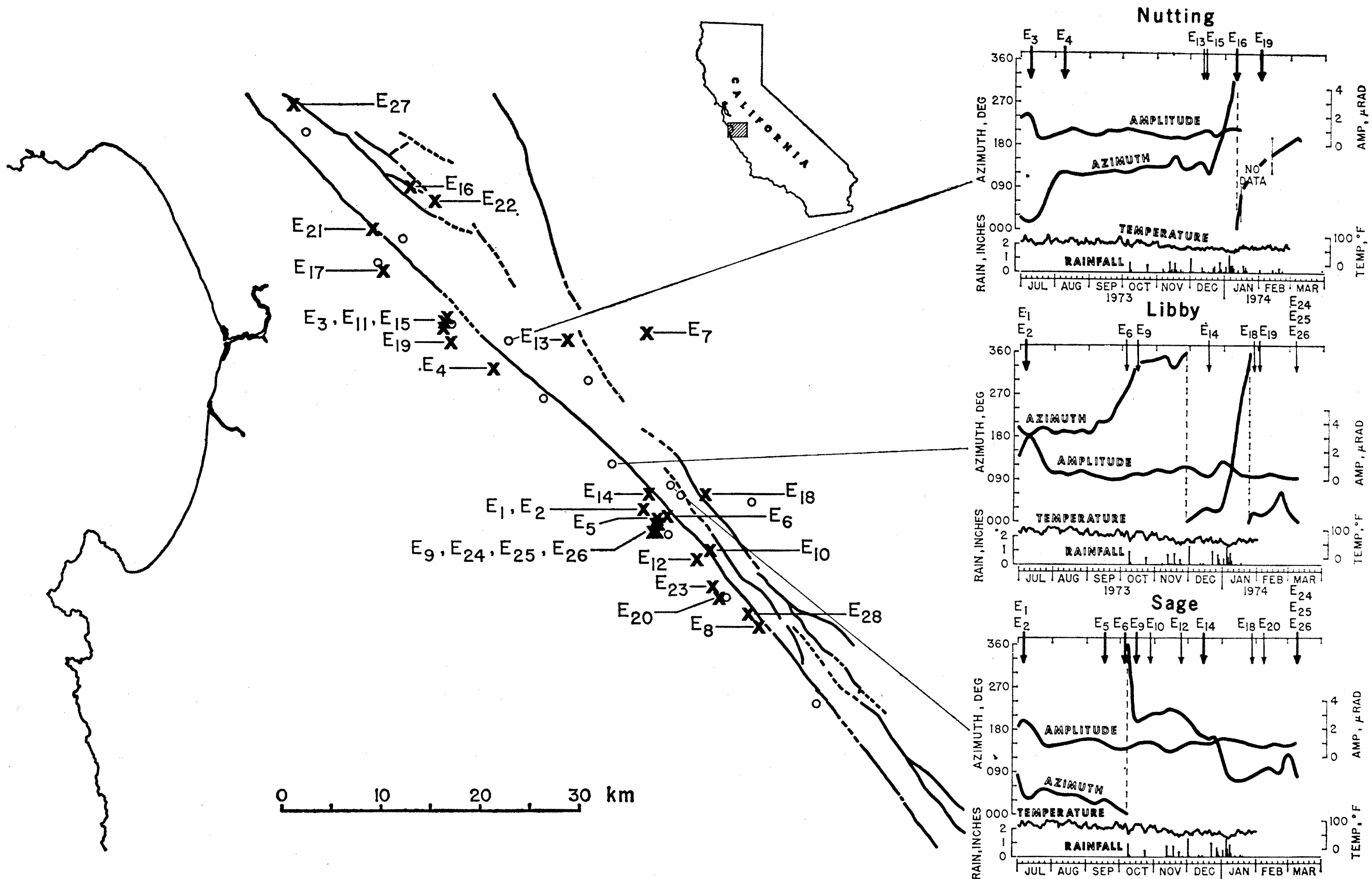

Fig. 2. Fault map of central California showing the 14 tiltmeter locations (open circles), all earthquakes ($M_L > 2.5$) that have occurred since July 1973 near these instruments (**X**), and the tilt, temperature, and rainfall records from the three tiltmeter sites that have been in operation the longest (Nutting, Libby, and Sage). The earthquakes E_1 to E_{28} are described in Table 1, and the occurrence times of the most significant earthquakes at each site are shown on the tilt history record of amplitude and direction of the change in the 7-day mean tilt vectors. The thickness of the arrows indicating earthquakes is proportional to 10 S/R, where R is the earthquake instrument distance. As discussed in the text, clear tilt changes apparently related to earthquakes are not easily distinguished at distances greater than 10 S.

tematic tilting of up to a microradian per month generally occurs in a particular fixed direction. However, prior to local earthquakes this direction can change grossly, and, after the earthquake, systematic tilt again occurs, although in a new fixed direction. This effect has been seen now for more than ten single events or groups of earthquakes, and no similar effect has been seen yet without the occurrence of an earthquake. Several such systematic changes in tilt have been seen on more than one instrument. An example of this behavior is shown in Fig. 1, which is a cumulative plot of the weekly mean tilt vectors for a site just southwest of Hollister. Also marked are major local earthquakes that occurred during this 8-month period. The rainy season started in mid-October. There is no obvious rainfall, pressure, or temperature dependence. Of particular interest is the tilt record after 26 December 1973, about 15 days before a $M_L =$ 4.3 earthquake 15 km to the northwest. During the time before the earthquake, the tilt vector reversed its direction completely, changing from a steady tilt to the southeast to one toward the earthquake in a northwesterly direction. After the earthquake the rotation continued, finishing finally, after a 360° rotation, where it had started.

4) Apparent short-period anelastic relaxation or aftercreep behavior of several different but systematic types has been seen simultaneously on up to five independent instruments after local earthquakes (*11*).

5) Some examples of short-period aseismic tilts with time constants of less than one-half to several hours have been observed with amplitudes of up to 0.5 μrad. Although similar in form to records of but not coincident with aseismic creep events, it seems likely that both types of events have the same origin.

The most important question about the earthquake mechanism is the location of the instrument with respect to an earthquake and the form of the tilt change with time that occurred. Figure 2 is a map of the general installation area showing the location of the tiltmeters and all earthquakes greater than $M_L = 2.5$ that have occurred since the tiltmeters have been operating. The pertinent data for these earthquakes are listed in Table 1. Also included in Fig. 2 are plots of amplitude and the direction of the change in the 7-day mean tilt vectors for the three tiltmeter sites that have been in operation the longest. All earthquakes such that a circle of radius equal to 12 S includes an instrument are plotted together with the temperature and rainfall records at these sites. The thickness of the arrow indicating an earthquake is proportional to 10 S divided by the earthquake instrument distance R and provides a crude method for rating the earthquakes at a particular site.

Although some of the less important earthquakes could perhaps be removed to simplify the records, for example, E_{13} and E_{15} from the Nutting record, E_9, E_{14}, and E_{18} from the Libby record, and E_{10}, E_{12}, E_{18}, and E_{20} from the Sage record, most earthquakes occur after periods of change in the tilt azimuth. The tilt amplitude records show no clear relation to earthquake occurrence. The Sage record from October to December is complicated by the number of events that occurred. However, from July to September no earthquakes occurred and the tilt azimuth record is flat. This is generally true also for the periods July to September and October to December 1972 on the Libby record, and from August to mid-December on the Nutting record.

The sense of the precursory azimuth change for the six earthquakes around the Nutting site is not clearly toward or away from the earthquake. For the 10 earthquakes at the Libby site the change is more often away from rather than toward earthquakes, and for the 13 events at the Sage site it is not clear that a preferred change exists. The precursor time T (in days) as a function of magnitude M does generally fit the relation

$$\log T = 0.8\ M - 1.9$$

derived by Whitcomb *et al.* (*3*), although we do not have a broad range of magnitudes.

A consideration of the general mechanism for earthquakes on the San Andreas fault is premature on the basis of these few initial though encouraging results. However, the four most striking features, listed below, place encouraging limits on the range of alternatives:

1) Earthquake-related tilt changes are more of a secondary or perturbation process on the local active crustal deformation near the fault.

2) The amplitude of surface tilt is larger than expected from simple elastic considerations, and appears not clearly related to earthquake occurrences.

3) The surface tilt direction is highly sensitive to the occurrence of local earthquakes.

Table 1. Occurrence times, locations, and magnitudes ($M_L > 2.5$) of the local earthquakes (E_1 to E_{28}) that have occurred since June 1973 in central California near the tiltmeter installations.

Earthquake No.	Date	Time (G.M.T.)	Latitude	Longitude	Depth (km)	Magnitude
E_1	July 5	1147	36°39.2′N	121°18.2′W	4.8	2.7
E_2	July 5	1702	36°39.2′N	121°18.1′W	5.5	3.0
E_3	July 9	2100	36°48.7′N	121°32.9′W	6.2	3.3
E_4	Aug. 7	0417	36°46.8′N	121°29.3′W	5.0	3.0
E_5	Sept. 17	0531	36°33.6′N	121°11.4′W	4.8	2.8
E_6	Oct. 4	0537	36°38.8′N	121°17.6′W	6.7	2.9
E_7	Oct. 6	0918	36°49.0′N	121°18.4′W	8.3	2.7
E_8	Oct. 12	1919	36°32.5′N	121°10.5′W	7.6	2.8
E_9	Oct. 14	1657	36°38.6′N	121°17.8′W	5.2	2.5
E_{10}	Oct. 27	2008	36°36.9′N	121°13.6′W	2.4	2.9
E_{11}	Nov. 15	0948	36°34.7′N	121°12.9′W	6.2	2.8
E_{12}	Nov. 24	0108	36°36.6′N	121°15.0′W	5.8	2.8
E_{13}	Dec. 13	0217	36°48.6′N	121°24.0′W	7.7	2.7
E_{14}	Dec. 14	1204	36°39.9′N	121°18.5′W	9.0	2.6
E_{15}	Dec. 14	2356	36°50.6′N	121°35.3′W	6.0	2.9
E_{16}	Jan. 10	1122	36°57.1′N	121°35.8′W	7.7	4.3
E_{17}	Jan. 23	1556	36°52.2′N	121°37.3′W	6.0	3.0
E_{18}	Jan. 27	1922	36°35.2′N	121°14.0′W	6.8	2.7
E_{19}	Feb. 1	0327	36°47.6′N	121°32.6′W	8.5	3.6
E_{20}	Feb. 7	1035	36°34.2′N	121°12.8′W	5.0	3.2
E_{21}	Feb. 8	0004	36°54.5′N	121°37.7′W	1.5	2.7
E_{22}	Feb. 8	0215	36°56.2′N	121°33.3′W	4.8	2.7
E_{23}	Feb. 20	1055	36°35.3′N	121°13.7′W	12.8	2.8
E_{24}	Mar. 8	1855	36°38.3′N	121°17.6′W	4.0	2.8
E_{25}	Mar. 8	1856	36°38.6′N	121°17.5′W	4.1	2.9
E_{26}	Mar. 8	1910	36°38.3′N	121°17.2′W	4.2	3.1
E_{27}	Mar. 16	1624	37° 1.1′N	121°43.6′W	9.7	3.0
E_{28}	Mar. 17	0029	36°33.5′N	121°10.6′W	3.5	2.5

4) The spatial extent of the surface deformation at tilt sensitivities of 10^{-7} radian rarely exceeds 10 *S*.

The simple model of deep aseismic slip along the fault, as indicated, for example, by the observed broad-scale heat flow anomaly (*12*), which has associated shallow seismicity and local crustal deformation effects, could explain some of the tilt observations.

It is difficult to use these observations to argue either for or against currently popular ideas of the dilatancy behavior of crustal rocks since tilts of either sense could result from dilatancy by causing variations in the depth of the dilatant region or by causing interaction with the stress fields around the fault. The simple form of large-scale positive crustal swelling does appear unlikely for the earthquakes we have seen. As more data become available, it will be possible to determine more uniquely details of the earthquake mechanism, in particular, whether similar effects occur for larger-magnitude ranges and for different locations.

M. J. S. JOHNSTON
C. E. MORTENSEN

U.S. Geological Survey, National Center for Earthquake Research, Menlo Park, California 94025

References and Notes

1. F. Press and W. F. Brace, *Science* **152**, 1575 (1966); T. Hagiwara and T. Rikitake, *ibid.* **157**, 761 (1967); T. Rikitake, *Tectonophysics* **6**, 1 (1968); E. F. Saverensky, *ibid.*, p. 17.
2. Y. P. Aggarwal, L. R. Sykes, J. Armbruster, M. L. Sbar, *Nature (Lond.)* **241**, 101 (1973); I. N. Gupta, *Trans. Am. Geophys. Union* **55**, 355 (1974); R. Robinson, R. L. Wesson, W. L. Ellsworth, *Science* **184**, 1281 (1974).
3. J. H. Whitcomb, J. D. Garmany, D. L. Anderson, *Science* **180**, 632 (1973).
4. A. Nur, *Bull. Seismol. Soc. Am.* **62**, 1217 (1972); C. H. Scholz, L. R. Sykes, Y. P. Aggarwal, *Science* **181**, 803 (1973).
5. M. A. Chinnery, *Bull. Seismol. Soc. Am.* **51**, 9 (1961); J. C. Savage, *J. Geophys. Res.* **76**, 1954 (1971).
6. C. E. Mortensen and M. J. S. Johnston, in preparation.
7. These units are manufactured commercially by the Autonetic Division of North American Rockwell, model 541B.
8. The installation procedure is similar to that described by R. V. Allen, D. M. Wood, and C. E. Mortensen [*Philos. Trans. R. Soc. Lond. Ser. A Math. Phys. Sci.* **274**, 219 (1973)].
9. M. J. S. Johnston, in preparation.
10. Estimates of source dimension as a function of earthquake magnitude have been made by M. Wyss and J. Brune [*Bull. Seismol. Soc. Am.* **61**, 1153 (1971)], and observations for San Andreas earthquakes have been made by W. Thatcher and T. Hanks [*J. Geophys. Res.* **78**, 8547 (1973)].
11. Very careful checking is necessary with this type of data to ensure that there is no possibility of an earthquake-induced instrumental effect.
12. A. H. Lachenbruch and J. H. Sass, in *Proceedings of the Conference on Tectonic Problems of the San Andreas Fault System*, R. L. Kovach and A. Nur, Eds. (Stanford Univ. Press, Stanford, Calif., 1973), p. 192.
13. We thank R. Allen and others at the National Center for Earthquake Research for useful suggestions and help.

15 July 1974

Aerosols in the Atmosphere: Calculation of the Critical Absorption/Backscatter Ratio

Abstract. *The ratio of the absorption coefficient to the backscatter coefficient for which heating and cooling effects due to aerosols exactly balance at the earth's surface has been calculated with the use of a radiative-convective atmospheric model. The results are compared with those obtained from several simpler mean radiative-transfer models.*

In this report a radiative-convective atmospheric (RCA) model (*1, 2*) is used to calculate the value of the aerosol extinction coefficient and also the magnitude of the critical aerosol absorption/backscatter ratio for which heating and cooling effects due to aerosols just balance to produce no net temperature change at the earth's surface. These quantities are calculated for three aerosol heights. The RCA critical ratios are compared with several other recent calculations obtained from simple mean radiative-transfer (MRT) models (*3–5*).

The RCA model results confirm (*2, 6*) that an aerosol layer in the atmosphere changes the radiative balance and produces two effects in the atmosphere: (i) an increase in the mean earth-atmosphere albedo (a cooling effect) and (ii) a reduction of the atmospheric radiative cooling (a heating effect). The aerosol backscatter of incoming solar radiation increases the earth-atmosphere albedo while the absorption of the solar radiation increases the atmospheric temperature (and thus reducing the net radiative cooling).

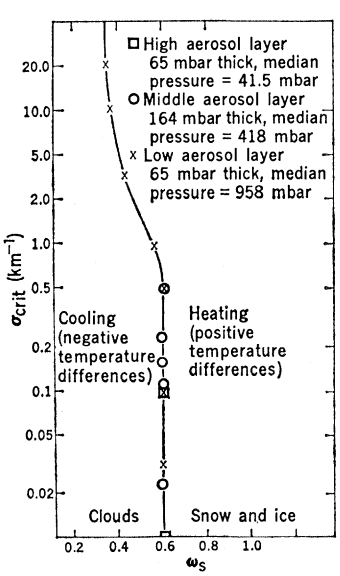

Fig. 1. Calculated RCA values of the critical aerosol extinction coefficient in the visible, σ_{crit}, as a function of the mean shortwave surface albedo, ω_s. The aerosol layer height (in millibars) is the median height for the particles.

The RCA model was developed by Manabe and Wetherald (*1*), and I have modified it to include an aerosol layer (*2*). A forward time integration of the solar and terrestrial flux imbalance is carried out until a radiative-convective, steady-state temperature is asymptotically approached at each of nine vertically aligned points in the atmosphere. A three-layer water cloud distribution with the appropriate optical properties (the same as that used by Manabe and Wetherald) is used to represent the clouds at 35°N in April. The physical distributions of H_2O, CO_2, and O_3 used by Manabe and Wetherald are also assumed, so that their necessary radiative-transfer effects can be included. The input aerosol optical parameters are similar to those previously used by Rasool and Schneider (*7*) for the global average aerosol. Parameterized expressions (*2*) are used to calculate (in a two-stream approximation) the fraction of transmitted and backscattered radiation due to the presence of the aerosol layer at various heights. Mie scattering is assumed for individual particles with a mean visible refractive index of $m = 1.50 - 0.1\ i$, an inverse fourth-power distribution of the particle radius, and a ratio of the mean extinction coefficient in the visible (0.55 μm) to that in the infrared (10 μm) of 0.108. Details of this model are given in (*2*). Earlier RCA model calculations (*2*) have shown that aerosols cause cooling at the earth's surface when the surface albedo, ω_s, is small ($\omega_s = 0.07$, as over water) and heating when the surface albedo is large ($\omega_s \geq 0.6$, as over snow).

These same calculations indicate that there is a value of the aerosol visible extinction coefficient, σ_{crit}, for which no heating or cooling occurs at the surface. This RCA model was used to compute the dependence of σ_{crit} on ω_s in the following way. A range of extinction coefficients, σ, and ω_s values was arbitrarily chosen,